

2023

Influence of Flanges Geometry on the Shear Behavior of Reinforced Concrete Inverted T-beams

Eman Shallan,

Follow this and additional works at: <https://digitalcommons.aaru.edu.jo/erjeng>

Recommended Citation

Shallan, , Eman (2023) "Influence of Flanges Geometry on the Shear Behavior of Reinforced Concrete Inverted T-beams," *Journal of Engineering Research*: Vol. 7: Iss. 2, Article 20.

Available at: <https://digitalcommons.aaru.edu.jo/erjeng/vol7/iss2/20>

This Article is brought to you for free and open access by Arab Journals Platform. It has been accepted for inclusion in Journal of Engineering Research by an authorized editor. The journal is hosted on [Digital Commons](#), an Elsevier platform. For more information, please contact rakan@aar.edu.jo, marah@aar.edu.jo, u.murad@aar.edu.jo.



Influence of Flanges Geometry on the Shear Behavior of Reinforced Concrete Inverted T-beams

Eman Shallan¹, Mahmoud A. Abdel-Aziz^{2*}, and Nesreen Kassem³

¹Master Student, Faculty of Engineering, Tanta University, Egypt

²Assistant Professor, Faculty of Engineering, Tanta University, Egypt – email: mahmoud.abdelaziz@f-eng.tanta.edu.eg

³Professor of reinforced concrete structures, Faculty of Engineering, Tanta University, Egypt.

Abstract- Most international codes of practice didn't consider the flange contribution of reinforced concrete T-beams in shear strength. In inverted T-beams loaded on the web, if the flange area is considered in shear strength, the results may be overestimated because after the web cracks open, the aggregate interlock which has a more significant contribution to shear decreases, and shear stresses tend to concentrate at the compression zone, which is located in the web of inverted T-beams. To quantify flange contribution, an experimental program backed by a finite element program based on a nonlinear 3D finite element model was carried out. The experimental program investigates the shear response of beams with varying flange geometry and reinforcement. The results showed that by increasing the flange geometry, the shear strength rises but up to a certain point, the contribution of the flange reinforcement to shear must be neglected. In the current analysis, the greatest contribution of flanges was determined to be 44.5% of total shear resisted by control beam without flange. Furthermore, the numerical model was utilized to visualize and quantify characteristics that are difficult to get experimentally, such as shear stress distribution between the web and the flanges. Also, the model was used to solve a matrix of beams to obtain the maximum shear resistance to make an accurate simplified computational model which shows good agreement with the experimental and finite element results.

Keywords- Shear strength, Shear tests, Flanges, Effective width, Reinforced concrete.

I- INTRODUCTION

Since the ambiguity of the phenomena involved, such as cracking-induced inhomogeneity, the relevance of the multi-axial stress states generated, the interaction between concrete and reinforcement, and the size effect involved with softening in compression or tension, shear strength of reinforced concrete members is challenging to predict. Many experimental and theoretical investigations have been carried out over several decades, resulting in significant breakthroughs in our knowledge of the shear resisting process [1], [2]. As a result, empirical and rational models capable of capturing experimental behaviour have been developed [3]–[11], some of which are being incorporated in concrete code design and assessment [12]–[14], despite the fact that the majority of them have been derived exclusively for members with a rectangular cross section.

Members with flanged cross sections (T-section, I-section, or box section) are highly common in modern building and bridge deck structures due to their excellent flexural strength/weight ratio. Shear is believed to be handled by the web via a truss mechanism. As a result, no flange contribution to shear strength is considered, which is assumed to be

completely resisted by the web via aggregate interlock anywhere along shear cracks.

Experiment results reveal that the shear strength of thin reinforced concrete (RC) beams [15]–[23] and slabs [24] with a T-shaped section is greater than that of beams with identical height, web width, and reinforcing quantity. For example, the beams with 300mm or larger flanges have approximately 25% higher ultimate strength compared with rectangular beams [25]. Also, for beams with constant web width, the larger the flange width, the greater the shear resistance, which can rise by up to 25% in comparison to the rectangular beam, even if shear resistance stays constant until a certain ratio flange width/web width. For the same web and flange widths, the thicker the flange, the greater the shear strength. Further, the flanges' impact to shear strength has already been identified and included in several theoretical models, such as those described in publications [26]–[35].

Based on the results of the aforementioned practical and theoretical study papers, it is possible to conclude that the compression flange makes a non-negligible contribution to the shear strength of beams with T-shaped sections, which is neglected in the shear specifications of current design codes. Neglecting such contributions in design is a conservative option that is widely accepted, despite being inaccurate. However, due to the growing number of infrastructures in operation that must be properly evaluated, assessing existing structures is becoming increasingly crucial. When used to the evaluation of existing structures, an overly cautious design technique may deem them unacceptably conservative, as is the case with many bridges now in operation that demonstrate a decent performance. As a result, a correct assessment of existing bridges and other transportation infrastructures, which are frequently designed with T-shaped cross section elements, necessitates a realistic evaluation of structural strength using models that include for the impact of flanges.

Because the shear loads transmitted by aggregate interlock are inversely proportional to the crack opening, hence shear transfer by aggregate interlock is only achievable at the crack tip. As a result, a significant portion of the shear stresses concentrate near the neutral axis, which is often situated in the flanges of T beams. Such stresses extend within the flanges in compression, decreasing in intensity as the distance to the web increases, as theoretically established by Ribas and Cladera [32], and Cladera et al. [33], following the model provided by Bairán and Mar [30], utilising a sectional model. As a result, no increase in shear strength is found at a particular value of flange width. A thicker flange, on the other hand, may distribute more shear loads and hence resist a larger shear force. This rise, however, diminishes gradually as the flange

depth increases, since shear stresses decrease with distance to the neutral axis owing to crack width growth.

Because most shear stresses at high loading levels concentrate around the neutral axis, a significant portion of them are placed in the uncracked compressed concrete zone, where compressive normal stresses owing to bending improve this region's ability to withstand shear. Furthermore, transverse reinforcement is commonly used in flanges to withstand shear lag and transversal bending. This type of reinforcement limits the concrete in the transverse direction, increasing the shear capacity of the T beam's compressed concrete zone.

Even while numerical models that use non-linear 3D-Finite element analysis [36], [37] may simulate such complicated processes, equations that take them into account in a simple but accurate way are required for rational and safe engineering assessment and design. The idea of "shear effective flanges width" was devised for this purpose, defined as a flange width that, assuming a constant shear stresses distribution in the transverse direction, would give the same shear force in the flanges as the real shear stresses distribution.

Placas et al. [17], Zararis et al. [29], Alberto Ayensa et al. [35], Ribas and Cladera [32], Cladera et al. [33], and Li et al [34] also used this notion in their shear strength models. Predictions of the outcomes of shear tests on T-shaped cross section beams done by Cladera et al. [33] demonstrated that accounting for the effective shear width yields less conservative and dispersed findings with regard to the measured result of ultimate shear. The dispersion achieved when estimating the shear strength of T beams, on the other hand, was significantly higher than when predicting the shear strength of rectangular beams. This suggested that, while the effective shear width is a valuable idea, its formulation requires further investigation in order to reflect the effects of the components involved and enhance the accuracy of shear strength estimates. In reality, the shear effective flanges width expressions used up to now do not account for flange confinement effects or the 3D passage of forces from the web to the flanges (shear lag effect), which must be captured by 3D finite element calculations.

Previous research ignored the existence of the flange on the tension side, which, according to what has been described, may be the worst scenario since the compressed area where shear resistance increases is in the web with the lowest dimension. However, another key element that may turn upside down is that the shear crack developed in the tensile side has a minor horizontal slope, which may result in the resistance of a greater number of stirrups and increases the crack path. These two opposing assumptions complicate the situation conceptually, and it must be subjected to experimental and finite element investigations to yield actual outcomes. Especially since these types of beams are used in the inverted beam raft foundations, transitional beams (columns are planted on them) and bridges, and they are elements with large loads. Experimental program backed by finite element program based on nonlinear 3D-FEA model were carried out. Once the model adjusted, the model was used to investigate the shear response of beams with varying flange geometry and transversal reinforcement. For this objective, the programme ABAQUS version 6.14 [38] was

employed. The numerical analyses provided data on the structural response that was difficult to measure experimentally, such as the distribution of shear stresses between the web and the flanges, which was very useful for quantifying the contribution of the web and the flanges on beams with different cross section geometry and longitudinal reinforcement.

II- HIGHLIGHTS

This study highlights the contribution of flange geometry and reinforcement in shear in case of RC inverted T-beams. A 3D-finite element model has been verified to match the experimental results for use by researchers and designers. The model was used to solve a matrix of beams to obtain the maximum shear resistance to make an accurate simplified computational model. A design expression was developed for computing the shear contribution of flanges in inverted T-sections.

III- TEST PROGRAM

A. Specimen design

Fig. 1 shows dimensions, longitudinal reinforcements detailing and cross section of the control beam B_0 (unit: mm). The shear capacity of the RC beam was somewhat lower than the bending capacity to ensure a shear failure, despite being designed in compliance with the design code for concrete structures [23]. As illustrated in Fig. 2a, the beam was 3000mm long with a clear span of 2800 mm, a total height of 400mm, and a web width of 200mm. The Beam have distinct bottom longitudinal reinforcement two layers of 2D16+4D18 and the top longitudinal reinforcement was 2D16. The web shear reinforcement consisted of 6mm stirrups placed 175 mm along the shear span and throughout the rest of the beam. The bottom concrete cover was 15mm thick. Test beams were monotonically tested up to failure under a four-point loading, with a shear span with a shear span-to-depth ratio of 2.5 ($a/d=890$ mm).

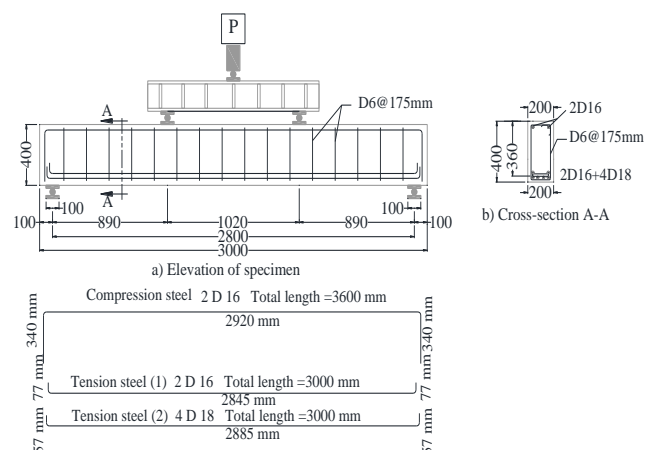


Fig. 1. Dimensions and reinforcement details of control beam B_0

B. Beams detailing and test program.

The control beam B_0 has a rectangular cross section, while the others have flange at the tension side (inverted T-beams).

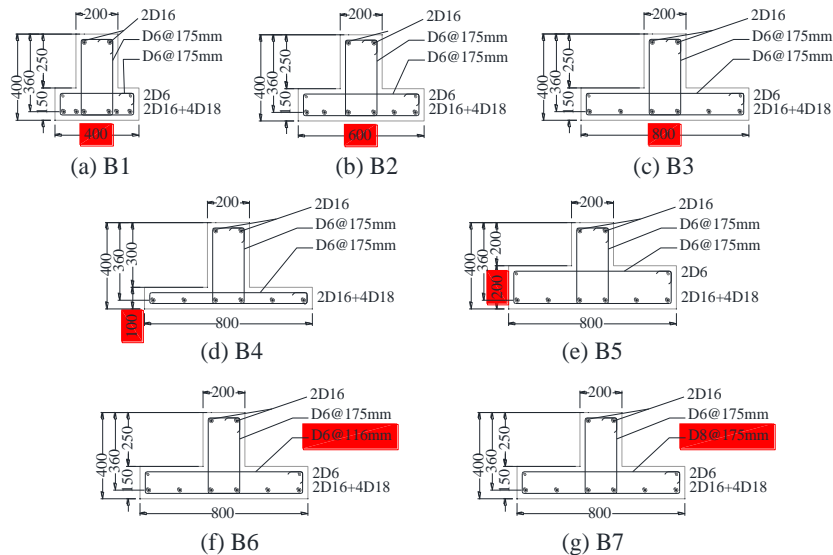


Fig. 2. Cross-section, dimensions, and reinforcement of test beams

Table 1: Experimental test matrix

beam	Flange width (mm)	Flange thickness	Stirrup in flange	Stirrup in web	Studied parameter
B0	200	-	-	-	D6@175mm Flange width effect Flange thickness effect Stirrup's area and spacing in flange
B1	400	150	D6@175mm	D6@175mm	
B2	600	150	D6@175mm		
B3	800	150	D6@175mm		
B4	800	100	D6@175mm		
B5	800	200	D6@175mm		
B6	800	150	D6@116mm		
B7	800	150	D8@175mm		

Other than the control beam, seven full-scale RC beams with inverted T-shaped cross-sections divided to investigate the shear response of beams with varying flange geometry (width and thickness), and transversal reinforcement in flange (Stirrups spacing in flange and bar diameter of the stirrups in flange). Table 1 and figures 2 show the beams test matrix and cross-section detailing.

Beams B₁, B₂, and B₃ were prepared to study the effect of flange widths of 400, 600, and 800 mm respectively on the beams shear behavior compared to the control beam B₀, figure 2a, 2b, and 2c. Beams B₄, B₅, and B₅ were produced to investigate the influence of flange thicknesses of 100, 150, and 200 mm on the beams shear behavior compared to the control beam B₀, figures 2d, 2e, and 2e. The web shear reinforcement is constant in all beams: 6mm stirrups placed 175 mm along the shear span and throughout the rest of the beam. In beams B₆ and B₇, the web shear reinforcement in the flange was D6@116 and D8@175 mm, respectively along the shear span and throughout the rest of the beam, figures 2f, 2g. These values were choice to study the effect of stirrups spacing and stirrups bar diameter in flange. The inverted T-beams beams have distinct bottom longitudinal reinforcement as beam B₀ except that the main longitudinal reinforcement was distributed in the flange in one layer with the same effective depth. The top longitudinal reinforcement also was constant. The concrete cover was 25mm thick to fix the effective depth in all beams.

C. Material properties

To prevent variances in the concrete strength of the tested beams, the same patch of ready-mixed concrete was put to each beam. The mixture proportions shown in table 2. Ordinary Portland R42.5 cement, limestone coarse aggregates with a nominal maximum size of 22 mm, and river sand with maximum size of 3 mm were used to prepare the concrete. The compressive strength of the concrete was measured using two sets of 300x150 mm cylinders. The beams and companion cylinders specimens were all cured outdoors for 28 days and kept wet by watering 1-2 times each day. On the test date for the beams, compression tests were done on standard cylinders with a 300 mm height and 150 mm diameter in accordance with ASTM C39/C39M. On the test day, the mean cylinder compressive strength (f_c) was 24.08. (The identified compressive cube strength was 30.1 MPa). Three cylinders were subjected to Brazilian tensile testing to ascertain their real tensile strength. The mean tensile strength at the time of the test was 2.93 MPa.

Table 3 shows the mechanical parameters of the reinforcement utilized in the test specimens resulted from uniaxial tensile testing on three steel bar specimens. For longitudinal reinforcement, the beams were reinforced with steel grade B500DWR (H.T.S) D18 and D16 mm deformed bars, and the stirrups were reinforced with steel grade 240/350 (N.M.S) D8 mm and D6 smooth bars. The table contains the average yield and ultimate strengths as well as the typical elastic modulus for the tested specimens.

Table 2: Mix proportions of materials (kg/m³) for cubic meter.

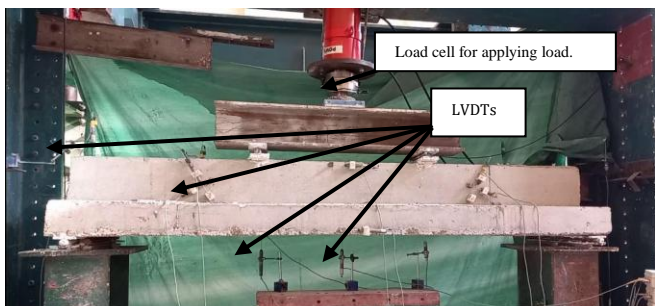
Water-to-binder ratio	Water	Coarse aggregate	Sand	Cement	f_c (MPa)	f_{cu} (MPa)	f_t (MPa)
0.50	180	1102	593	360	24.08	30.1	2.93

Table 3: Steel reinforcement's characteristics.

Diameter, mm	Yield strength, (MPa)	Ultimate strength, (MPa)	ϵ_y	ϵ_u	E_s ($\times 10^5$ N/mm ²)
6	268	369	0.0013	0.168	2.04
8	274	365	0.00134	0.178	2.05
16	528	723	0.00256	0.132	2.05
18	534	727	0.00262	0.138	2.04



(a) Installation of reinforcing mesh inside the formwork (b) a final view before casting concrete

Fig. 3. Fabrication and preparation of test beams**Fig. 4. Test setup**

D. Fabrication and preparation of test beams

Care has been taken to cast the beams in conformity with site work so that the form work of the slab was fixed at the bottom and the beam web was inverted to the top. Figure 2 a show the installation of reinforcing mesh inside the formwork and figure 2b shows a final view before casting concrete.

E. Loading program and instrumentations

Figure 4 depicts the test equipment utilised in this experimental work. The simply supported RC beams were subjected to four-point loading in order to get the load-deformation curves under a monotonically increasing load till failure. The load was delivered to the tested beam through a transfer steel beam and a hydraulic jack with a maximum capacity of 3000 kN. Each beam was loaded symmetrically about the centreline and had a shear span-to-depth ratio of 2.5 ($a/d=890$ mm). The initial loading rate was 1.0 kN/s, however it dropped to 0.33 kN/s after yielding. The load cell, which was attached to the load piston, was used to record the applied load. There are nine LVDTs for each beam (linear variable differential transducers). Five of them were mounted to measure vertical deformations: one at midspan, two at the

loading sides, and two at the supports. To calculate the shear deformations of the shear critical sections, two LVDTs are attached perpendicular to the line linking the loading point and support on each side of the beam (which is almost the direction of diagonal cracks). An automated data acquisition system attached to a laptop through a USB connection was utilised to record the loads, displacements, and deformations. A second crack width calibrated tool was utilised to measure the crack width of the beam during loading. The load was increased and at specific points the loading was stopped, and the crack propagation was drawn. At the end of the test, full crack patterns were available. The test was stopped when the load dropped by logical failure of the beam.

IV- EXPERIMENTAL RESULTS

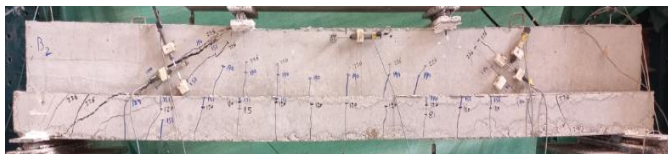
Table 4 contains a summary of the most important laboratory results, calculated initial stiffness and absorbed energy.

A. Failure modes

All beams collapsed due to shear compression failure. The shear compression failure mechanism was identical to the normal failure mechanism employed in shear analysis of reinforced concrete beams in case of rectangular section, but the crack pattern was somewhat different in the case of a flanged beams. In control beam B_0 , the diagonal first shear crack developed at the centre of shear span parallel to the delusory line connected the load and the support. Then with load increase, the crack spread to the longitudinal tension bars and began running along their length, causing dowel action. The opposite tip of the crack went all the way to the compression zone. This crack looked to be caused by the diagonal tension splitting combined forces whereby load increase the width of the crack increased up to failure. Figure 5a depicts the crack patterns after failure for B_0 .

In case of beams B_4 , no effect was observed for the presence of the flange, and the beams behavior was close to the control beam, figure 5d. This is most likely owing to the flange's lack of rigidity, since the section behaved under load as if it were a rectangular section without a flange. In case of inverted T-beams, figure 5a to 5h except 5d, a diagonal tension crack developed in the web in the same manner of B_0 . By load increase the crack spread to the web interface in compression zone and the opposite end of the crack went towards the tension flange. By load increase the tension flange showed a synergistic action with the web to resist shearing and delaying running of shear crack along their length to the longitudinal bar. Near the ultimate load the beams failed with a crack appeared on the edge of the flange. This crack looked to be caused by diagonal tension splitting in the flange.

**(a) Crack patterns of B_0**



(b) Crack patterns of B₁



(b) Crack patterns of B₂



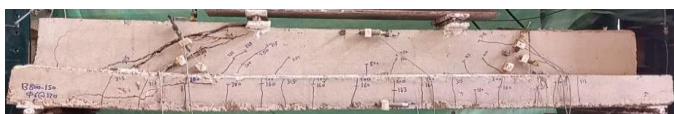
(c) Crack patterns of B₃



(d) Crack patterns of B₄



(e) Crack patterns of B₅



(g) Crack patterns of B₆



(h) Crack patterns of B₇

Fig. 5. Crack patterns of test beams

B. Flexural cracking load.

Figure 6 shows the effect of flange geometry t_s and B_f and transversal reinforcement on first flexural cracking load. The first flexural crack occurred in beam B₀ at 63 kN (22% of the ultimate load). The first flexural crack occurred at 81, 97, and 136 kN (20.6%, 24.1%, and 32.5% of the ultimate load) for beams B₁, B₂, and B₃, respectively. It is clear that extending the width of the tension flange delayed the appearance of the

first flexural crack due to increasing the cross-section inertia. When the flange width was increased to $2b_w$, $3b_w$, and $4b_w$, the first cracking load increased by 29%, 54%, and 116%, respectively. For beams B₄, B₃, and B₅, the first flexural crack developed at 98, 136, and 166 kN (28.2%, 32.5%, and 32.3% of the ultimate load, respectively). It is obvious that increasing the tension flange thickness delayed the formation of cracks, resulting in an increase in the magnitude of the first flexural cracking load. When the flange thicknesses were increased to $0.25t_b$, $0.375t_b$, and $0.5t_b$, the first flexural cracking load increased by 56%, 116%, and 163%, respectively.

At about the same stress as B₃, the first flexural crack occurred in beams B₆ and B₇ (between 133 and 136 kN). That is, the change in flange transversal reinforcement has no effect on the initial first cracking load and this is logic.

C. Initial stiffness

The data in figure 7 shows that the initial stiffness of B₁, B₂ and B₃ have significant increased compared to the control beam B₀ by 14%, 24% and 32%, respectively. Also, the data indicates that the initial stiffness of B₄, B₃, and B₅ has risen by 13%, 32%, and 52%, respectively, when compared to the control beam B₀. It indicates that the initial stiffness of inverted T-beams increased obviously with the increase of flange geometry (t_s or B_f). The initial stiffness of B₃, B₆ and B₇ almost the same because the initial stiffness of the beam is mainly affected by concrete geometry of the beam where the elastic modulus of the beams was almost equal due to the negligible effect of transversal steel.

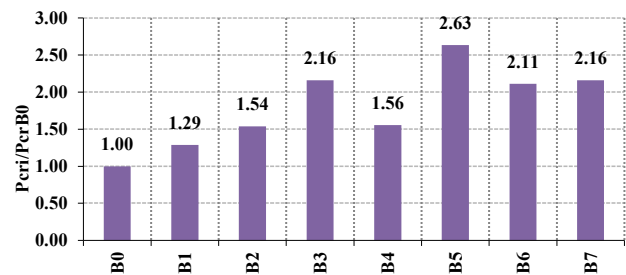


Fig. 6. Effect of flange geometry and transversal reinforcement on first flexural cracking load

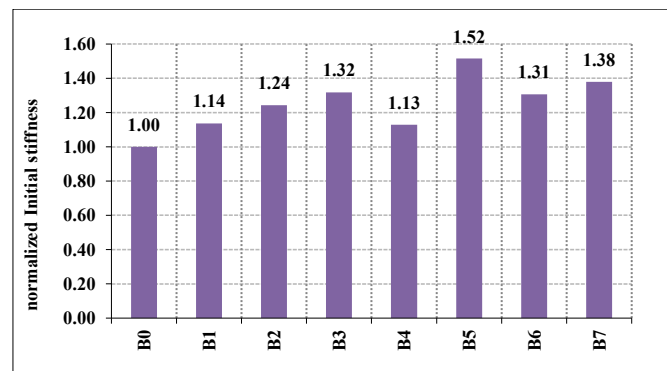


Fig. 7. Effect of flange geometry and transversal reinforcement on initial stiffness

D. First shear cracking load.

Figure 8 shows the effect of flange geometry t_s and B and transversal reinforcement on first shear cracking load. In beam B_0 , the diagonal first shear crack developed at 156 kN (54.75% of the ultimate load).

For beams B_1 , B_2 and B_3 , the first shear crack developed at 189, 230, and 260 kN (48.1%, 57.2%, and 62.2 % of the ultimate loads) respectively. It is evident that by increasing the width of the tension flange, the appearance of the first shear crack was delayed with a significant improvement in the value of the first shear cracking load. The initial shear cracking load rose by 21%, 47%, and 67% when the flange width was raised to $2b_w$, $3b_w$, and $4b_w$, respectively.

The first shear crack occurred at 164, 260, and 293 kN (47.3%, 62.2%, and 57% of the ultimate load) for beams B_4 , B_3 , and B_5 , respectively. It is clear that expanding the thickness of the tension flange delayed the emergence of the first shear crack, resulting in an increase in the value of the first shear cracking load. It is clear that the effect of the flange thickness the case of small thicknesses ($t_f/t_b \leq 0.25$) is almost negligible, while the observed load at the first crack improved in the case of large thicknesses ($t_f/t_b \geq 0.375$).

The initial shear cracking load rose by 5%, 67% and 88% when the flange thicknesses was raised to $0.25t_b$, $0.375t_b$, and $0.5t_b$, respectively.

The first shear crack in beams B_6 and B_7 was developed at almost near the load of B_3 (between 252 and 257 kN). Which means that the variation in flange transversal reinforcement has no influence on the initial shear cracking load.

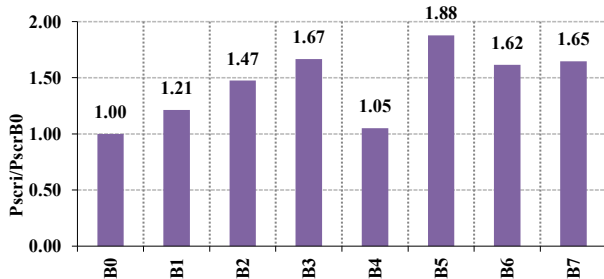


Fig. 8. Effect of flange geometry and transversal reinforcement on first shear cracking load

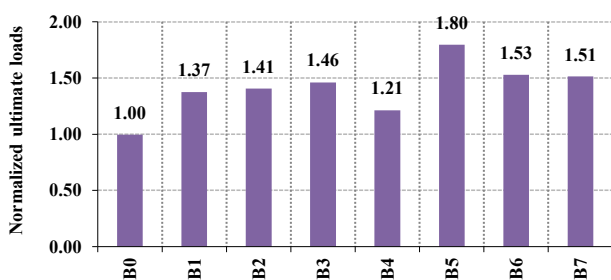


Fig. 9. Effect of flange geometry and transversal reinforcement on the ultimate shear capacity

E. Ultimate load

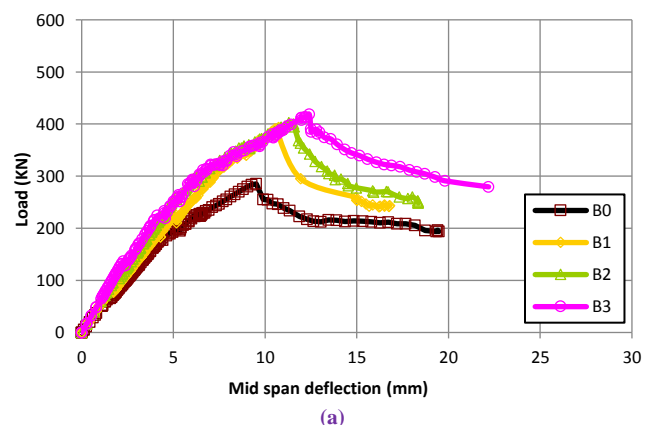
The ultimate shear capacity of every beam B_1 , ... to B_7 compared to the control beam B_0 are listed in figure 9. As demonstrated in the figure, employing the flange dimensions

(thickness and width) greatly increased the shear capacity of the reinforced beams. The ultimate shear capacity reached 285, 393, 402, and 418 kN for beams B_0 , B_1 , B_2 , and B_3 , respectively. It is clear that extending the width of the tension flange delayed the emergence of failure while significantly improving the value of the ultimate shear capacity. When the flange width was increased to $2b_w$, $3b_w$, and $4b_w$, the ultimate shear capacity load increased by 37%, 41%, and 46%, respectively.

For beams B_0 , B_4 , B_3 , and B_5 , the ultimate shear capacity reached 285, 347, 418 and 514 kN, respectively. It is obvious that increasing the tension flange thickness delayed the failure, resulting in an increase in the magnitude of the ultimate shear capacity. It is obvious that the influence of flange thickness is essentially minimal in the case of small thicknesses ($t_f/t_b \leq 0.25$), where the increase in the ultimate load at this value was only 21%, but the measured ultimate load enhanced in the case of big thicknesses ($t_f/t_b \geq 0.375$). The ultimate shear load rose by 46% and 80% when the flange thicknesses was raised to $0.375t_b$, and $0.5t_b$, respectively. The ultimate shear capacity showed a slight increase by decreasing the spacing between the transversal steel or increasing the transversal bar diameter. The gain was only 4.6% when decreasing the spacing from 175 mm to 116, and the gain was only 3.6% when increasing the bar diameter from D6 to D8. Thus, the variation in flange transversal reinforcement has negligible influence on the ultimate shear capacity.

F. Load deflection response

Figure 10 depicts the load-deflection curve of the tested beams. For comparison, the response of the reference beam B_0 was provided. As shown in Fig. 10a 10b and 10c, from the beginning up to failure, there was significant difference in load-deflection response between the reference beam B_0 and other compared beams. From the beginning up to the first shear crack, the effect the flange geometry and reinforcement was clear in the resist of higher deflection at the same load level. Approximately at 266kN for example, the deformation in all beams except B_5 was close, where the control beam had a large deflection. Beam B_5 which has the maximum flange dimensions shows the highest resistance to deformations up to its failure load. Also, after reaching the ultimate load, the control beam failed suddenly, but existence of flange reduces the severity of the sudden collapse.



(a)

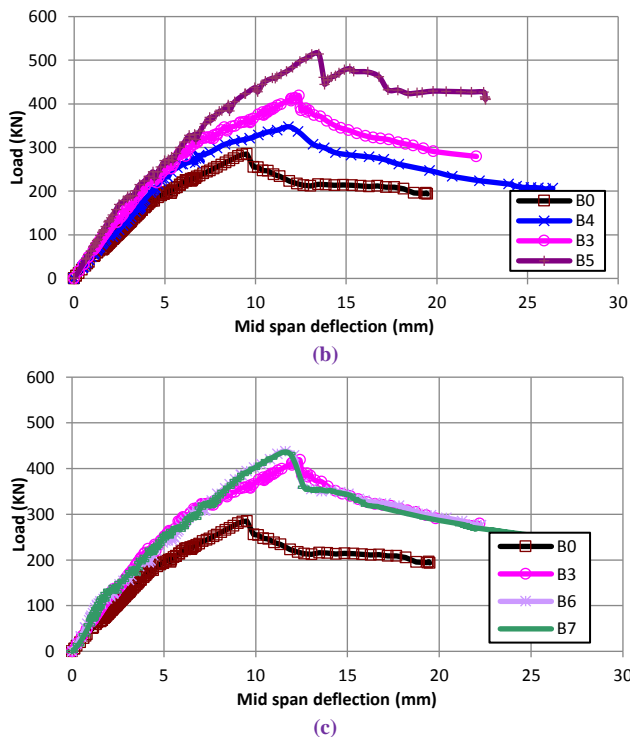


Fig. 10. Effect of flange geometry and transversal reinforcement on the ultimate shear capacity

G. Energy absorption

Various measurements have been used in previous studies to assess ductility [39]. One of the most significant indications was ductility as measured by energy absorption. The area under the load-deflection curves up to the maximum load (E) represents the energy absorption (E). The lowest value was obtained by the control beam B₀, as predicted. Figure 11 shows normalized energy absorption values compared to the control beam. The increase in energy absorption reached about 53%, 69%, and 103% in beams B₁, B₂, and B₃ respectively compared to the control beam B₀. Whereas the beams showed a great enhancement in energy absorption when the flange width exceed 3b_w. In comparison to the control beam B₀, the increase in energy absorption was approximately 57%, 103%, and 172% in beams B₄, B₃, and B₅. When the flange thickness exceeded 0.375t, the beams showed a significant increase in energy absorption. The variation in flange transversal reinforcement has negligible influence on energy absorption.

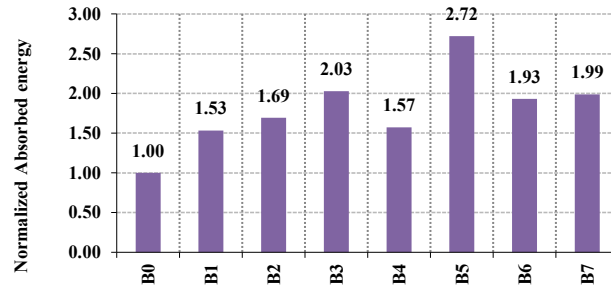


Fig. 11. Effect of flange geometry and transversal reinforcement on the absorbed energy

V- FINITE ELEMENT PROGRAM.

A. Description of finite element model

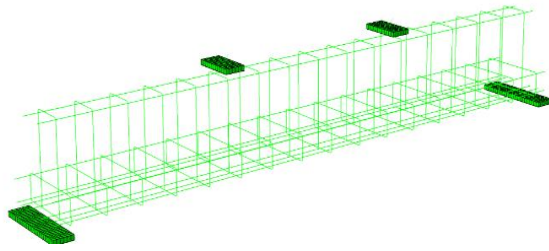
Figure 12 depicts the finite element model of the reinforced concrete beam by Abaqus [40]. The mesh of concrete mass, which is regarded as a homogenous solid, is created using the 8-node linear brick element "C3D8R" of Abaqus, with limited integration and hourglass control. In contrast, 2-node linear beam elements "B31" of Abaqus are used to form the mesh of reinforcement bars with circular cross sections whose diameter is equal to the diameter of the corresponding corrugated bars. Furthermore, as embedded elements, these beam elements interact with the concrete ones.

The mechanical behavior of the concrete brick components was assumed to be isotropic, and concrete damage was accounted for using an Abaqus damage-plasticity model in both compression and tension. In contrast, the mechanical behavior of the reinforcing beam components investigated is both isotropic and elastic-plastic. The mechanical properties of materials were determined based on the test results reported. The linear and non-linear material constitutive curves were employed, as well as the damage criteria. The model included in Abaqus for failure mechanism is a continuum, plasticity-based concrete damage model. Based on the total stress tensor, it is believed that the principal two failure modes of the concrete material are tensile cracking and compressive crushing.

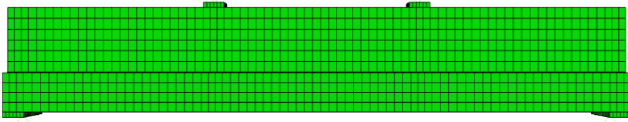
The boundary conditions of the finite element model were elastic supports applied to beam area nodes in contact with the elastomeric bearing pads and a pressure load applied to beam area nodes where the test load operates.

Table 4: Experimental results, calculated initial stiffness and absorbed energy

beam designation	Experimental results						Initial stiffness (kN/mm)	Absorbed energy
	Flexural cracking load (kN)	First shear cracking load (kN)	Ultimate load (kN)	Deflection at cracking (mm)	Deflection at first shear cracking load (mm)	Deflection at ultimate load (mm)		
B ₀	63	156	285	1.38	3.74	9.52	45.65	1459.8
B ₁	81	189	393	1.56	4.2	10.74	51.92	2238.8
B ₂	97	230	402	1.71	4.49	11.29	56.73	2473.1
B ₃	136	260	418	2.26	5.29	12.4	60.18	2962.5
B ₄	98	164	347	1.9	3.67	11.8	51.58	2295.9
B ₅	166	293	514	2.4	5.8	13.49	69.17	3969.8
B ₆	133	252	437.5	2.23	5.6	11.6	59.64	2821.1
B ₇	136	257	433	2.16	5.22	11.85	62.96	2903.7



(a) Elements of reinforcement, loading plates and supports



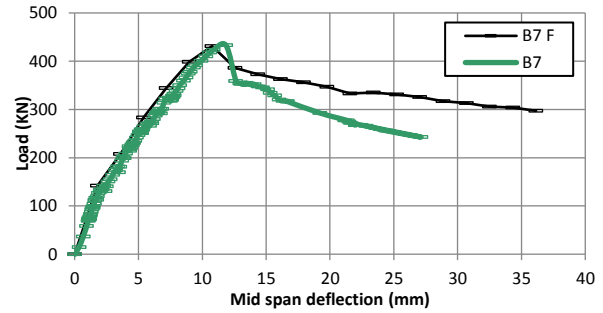
(b) Solid elements and mesh detail

Fig. 12. FE model of the reinforced concrete beam

B. Calibration of finite element model with experimental results

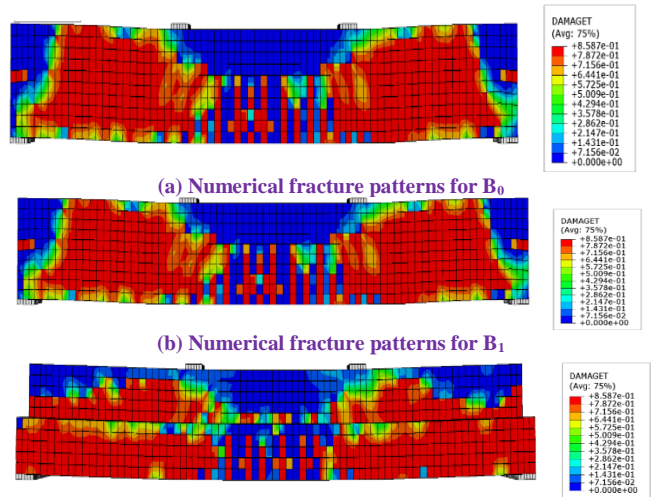
Figure 13 depicts the load versus the vertical mid-span displacement for both the experimental tests and the numerical simulation for B₂, B₃, and B₇. Figure 14 depicts the experimental and numerical fracture patterns for B₀, B₁ and B₅.

According to the study, the 3D nonlinear Finite Element model was able to predict the experimental response of inverted T-beams accurately when subjected to shear tests. However, there was a notable difference between the model and experimental results - the model consistently showed higher stiffness compared to the actual tests.



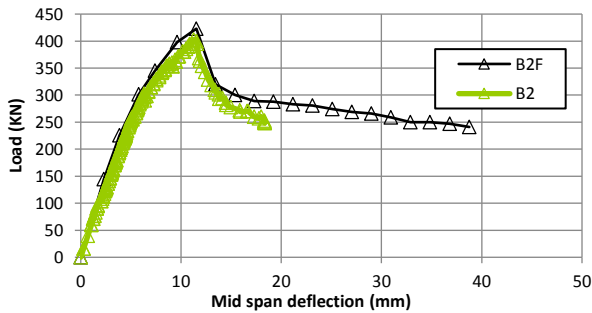
(c) Load mid span deflection in experimental findings and finite element for B₇

Fig. 13: Load mid span deflection in experimental findings and finite element

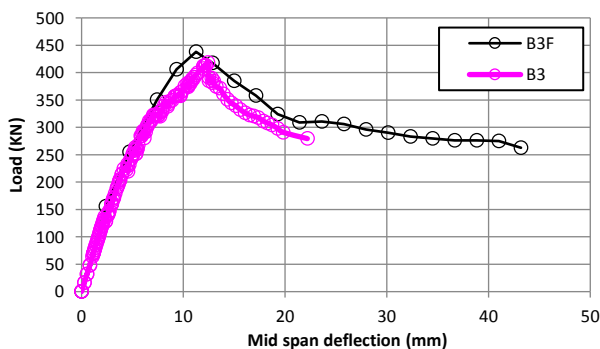


(c) Numerical fracture patterns for B₅

Fig. 14. Numerical fracture patterns for B₀, B₁ and B₅



(a) Load mid span deflection in experimental findings and finite element for B₂



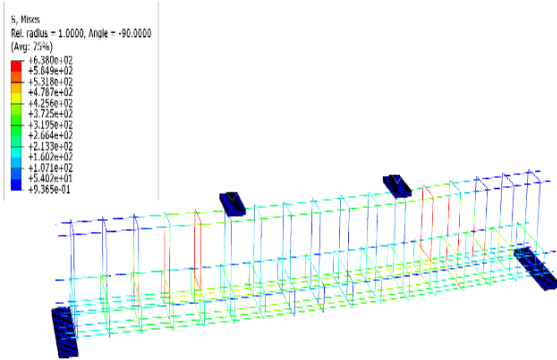
(b) Load mid span deflection in experimental findings and finite element for B₃

This discrepancy could be attributed to several factors, such as the assumptions made in the model, the accuracy of the material properties used, or the testing conditions. Further analysis and refinement of the model may be necessary to improve its accuracy and better align it with the experimental results. Nonetheless, the study demonstrates the potential of using such models to simulate and predict the behavior of structural elements under different loading conditions. In general, the model demonstrates a very excellent agreement.

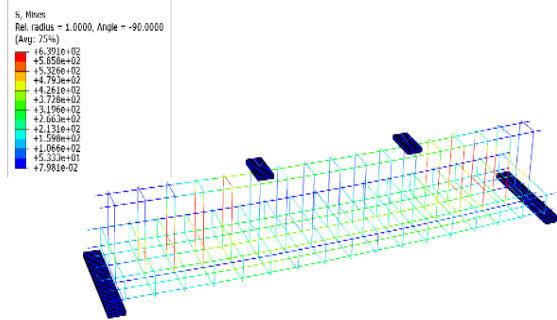
Figure 14 shows the steel stress for R.C beams B₁, B₂, and B₃ respectively. By comparing the results, it seems that the contribution of transverse reinforcement in flanges at vertical parts decreases rapidly with increasing flange width. Thus, the stress in the transversal steel located at a distance of more than 3b_w should be neglected in calculating the shear contribution of the flanges.

Also as shown in figure 15 from steel response, as the flange width increases, the shear contribution of the concrete in flanges decrease. However, it should be noted that for large flange widths, the shear stresses tend to concentrate around the web and the web reinforcement, and their extension into the flanges is limited. But from figure 16, It is important to note that this trend is not observed as the depth of the flanges increases.

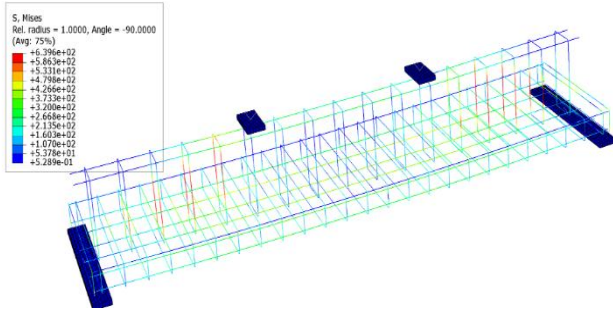
One of the objectives of the study is to use a three-dimensional model to solve an integrated matrix of variables related to the same variables studied in the experimental study. The model was used to solve a matrix shown in table 5 of R.C. inverted T-beams to obtain the maximum shear resistance to make an accurate simplified computational.



(a) Numerical steel stress for B₁

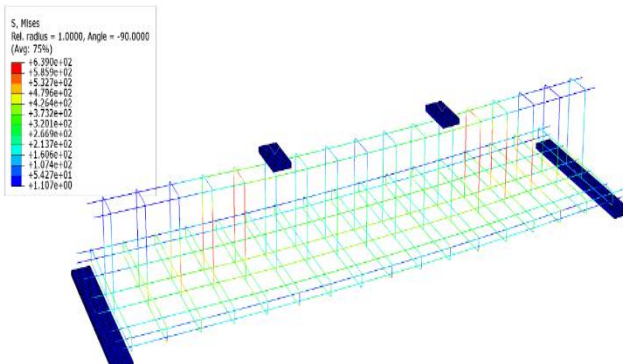


(b) Numerical steel stress for B₂

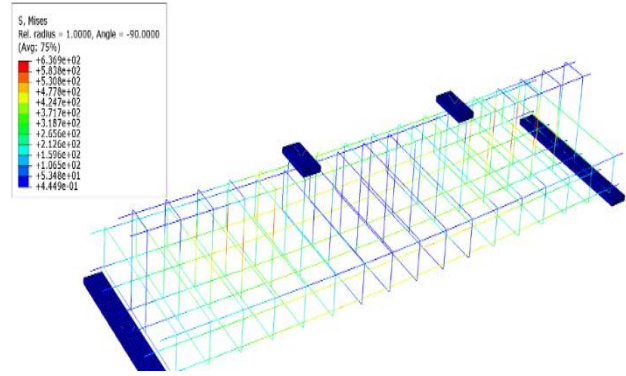


(c) Numerical steel stress for B₃

Fig. 15: Numerical steel stress for B₁, B₂, and B₃



(a) Numerical steel stress for B₄



(b) Numerical steel stress for B₅

Fig. 16: Numerical steel stress for B₁, B₂, and B₃

Table 5: matrix of parametric study for ultimate capacities for combined parameters.

d _r /d	B _f /b _w		
	2	3	4
0.139	336 kN	353 kN	361 kN
0.278	402 kN	423 kN	438 kN
0.417	481 kN	494 kN	503 kN

VI- CALCULATION OF ULTIMATE CAPACITY OF INVERTED T-SECTION

The ultimate shear capacity of the RC beams may be calculated by adding the shear capacities of the concrete web section (b_w.d), and web reinforcement, as shown in Eq. (1).

$$V_u = V_{web} + V_s \tag{1}$$

where V_u = ultimate shear capacity, V_{web} = shear capacity of concrete web; and V_s = shear capacity of web reinforcement

To estimate the shear strength of concrete web section, ACI-318 [41] provided the following equation:

$$V_c = \frac{1}{6} \sqrt{f'_c} \cdot b_w \cdot d \tag{2}$$

where f'_c = cylinder concrete compressive strength, b_w = beam width, and d = effective beam's depth

The second contribution is the action of internal reinforcement. This contribution might be estimated using the following formula:

$$V_s = \frac{A_{st} \cdot f_{ys}}{s} d \tag{3}$$

where A_{st} is the total stirrups area in web, f_{ys} is the yield strength of stirrups, s is the spacing between stirrups, and d is the section depth.

It is evident from Table 6 that the ratio between the experimental and calculated load for the reference beam is 1.58. This is acceptable because the international codes are keen that their equations for calculating the ultimate shear capacity for the R.C sections less by a good margin as a result of the brittle collapse by shearing, and the lack of sufficient indicators (cracks and deformations) before the failure. The increase between the experimental and calculated load in samples B₁ to B₇ ranged from 93% to 186% due to the contribution of the flange.

Table 6: Prediction model and finite element versus the experimental results.

Beam	Experimental V_{exp}^* (kN) = $V_{exp}/2$	Analytical			$V_{exp}^*/V_{T Aci}$	Experimental $V_{ex, flange}$	Experimental flange participation with safety margin $V_{ex, flange}/1.58$	V_{flange} By equation (4)	$\psi = \frac{v_{ex, flange}/1.58}{V_{flange by eq.4}}$
		$V_{web, Aci}$ (KN)	$V_{s, Aci}$ (KN)	$V_{T Aci}$					
B ₀	142.5	58.79	31.16	89.95	1.584	---	---	---	---
B ₁	196.5				2.18	54	34.1	37.47	0.910
B ₂	201				2.23	58.5	37	48.98	0.755
B ₃	209				2.324	66.5	42	73.48	0.572
B ₄	173.5				1.93	31	19.6	48.98	0.400
B ₅	257				2.86	114.5	72.46	97.97	0.740
B ₆	216				2.4	73.5	46.5	73.48	0.633
B ₇	224.5				2.495	82	51.9	73.48	0.706

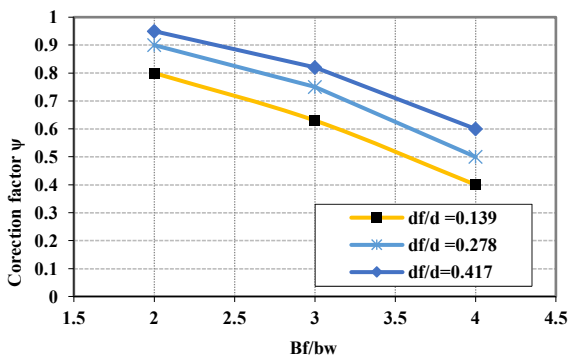
The contribution of the flange was considered after dividing its actual contribution in shearing by 1.58, which is the ratio between the experimental and calculated load of the reference beam B₀ to maintain the same principle adopted by international codes in the difference between theoretically calculated results and laboratory results. To predict the flange contribution, use the same formula in equations 2 and 3 with flange dimension. The participation in shear force in ultimate shear capacity by the flange may be calculated by adding the shear capacities of the concrete web section $((B_f - b_w) \cdot d)$, and web reinforcement in the flange, as shown in Eq. (4). The participation of steel in the flange is considered for steel in width not more than $3b_w$ only. The results are shown in the last column in table 5.

$$V_{flange, act} = \left(\frac{1}{6}\sqrt{f'_c} \cdot (B_f - b_w) \cdot d_f + \frac{A_{stf} \cdot f_{ys}}{s} d\right) \quad (4)$$

A contribution factor with an improved value through laboratory and finite element results may be added to equation (4) and the equation become:

$$V_{flange} = \psi \left(\frac{1}{6}\sqrt{f'_c} \cdot (B_f - b_w) \cdot d_f + \frac{A_{stf} \cdot f_{ys}}{s} d\right) \quad (5)$$

where ψ is the flange contribution factor and curve 17 gives this value according to d_f/d and B_f/b_w . this curve is built on the regression analysis to match the shear capacity with the experimental results and finite element results.

Fig. 17: Value of flange contribution factor ψ used with equation (5)

Solved example:

Calculate the expected experimental ultimate shear capacity for a simple supported inverted T-beam tested under four-point loading. The total web dimension is 500 mm x 250 mm, the total flange dimension is 800 mm x 180 mm, the concrete

cover is 40 mm, and D8@120 mm shear reinforcement. Cylinder concrete compressive strength is 26 MPa and the yield strength of stirrups is 260 MPa.

Solution:

$f'_c = 26$ MPa, $f_{ys} = 260$ MPa, $b_w = 250$ mm, $d = 460$ mm, $A_{st} = 56.5$ mm², $B_f = 800$ mm, $d_f = 140$ mm, $A_{stf} = 56.5$ mm², and $s = 120$ mm,

From equation 1, 2 and 3 calculate the web contribution:

$$V_s = \left(\frac{1}{6}\sqrt{26} \times 250 \times 460 + \frac{56.5 \times 260}{120} \times 460\right) / 1000 = 154 \text{ kN}$$

Form the Fig. 17 get the flange contribution factor with $B_f/b_w = 800/250 = 3.2$ and $d_f/d = 140/460 = 0.304$

$$\psi = 0.72$$

Because $B_f > 3b_w$ the web reinforcement in flange did not contribute to resist shear force and the flange contribution can be calculated from equation 5 by neglecting reinforcement term:

$$V_{flange} = \frac{0.72 \left(\frac{1}{6}\sqrt{26} \times (800 - 250) \times 140\right)}{1000} = 47.1 \text{ kN}$$

The total analytical shear force = $154 + 47.1 = 201$ kN

The expected experimental ultimate shear capacity = $1.58 \times 201 = 317$ kN

VII- FUTURE STUDIES NEEDED

Study the influence of flanges geometry on the shear behaviour of reinforced concrete inverted:

1. T-wide beams.
2. T-deep beams.
3. T-large spans beams.
4. T-beams with concentrated steel in web

VIII- CONCLUSION

Based on the experimental and numerical analyses conducted, the study has revealed that the shear resistance at the ultimate stage is not dependent only on the compression zone's area in the section. However, it should be noted that the tension flanges (i.e., the flanges of inverted T-section) also play a role in resisting shear stress along with the web. This suggests that the contribution of the tension flanges should be considered when evaluating the overall shear resistance of the section. By taking into account the combined contribution of all components of the section, a more accurate assessment of



its shear strength can be made. Also, it is possible to derive the following conclusions:

1. As the width and depth of the flanges increase, the flexural cracking load, the first shear cracking load, and the amount of shear force carried by the flange also increased. However, it should be noted that for large flange widths, the shear stresses tend to concentrate around the web, and their extension into the flanges is limited. It is important to note that this trend is not observed as the depth of the flanges increases.
2. The area of transversal reinforcement in flanges had a negligible effect on the first cracking load, the first shear cracking load, deformations, and the ultimate load but the finite element model showed that transversal reinforcement increases the shear force carried by flanges up to a distance not more than three times the web width.
3. According to the study, the 3D nonlinear Finite Element model was able to predict the experimental response of inverted T-beams accurately when subjected to shear. However, there was a notable difference between the model and experimental results that the model consistently showed higher stiffness compared to the actual tests.
4. An accurate simplified computational model was suggested based on the experimental and finite element results showing good prediction to the ultimate capacity.

Authorship contribution statement: **Eman Shallan:** Implementation of the experimental program, collecting data curation data, writing original draft, **Mahmoud Abdelaziz:** Auxiliary in experimental program, Conceptualization data curation, review original draft, and editing, **Nasreen Kassem:** Supervision & review final draft.

Funding: The authors state that this research has not received any type of funding.

Conflicts of Interest: The authors should explicitly declare if there is no conflict of interest.

REFERENCES

- [1] "Vecchio FJ, Collins MP. The modified compression-field theory for reinforced concrete elements subjected to shear. *ACI J* 1986;83(2):219–31."
- [2] "Muttoni A, Ruiz MF. Shear strength of members without transverse reinforcement as function of critical shear crack width. *ACI Struct J* 2008;105(2):163–72."
- [3] "Marí A, Bairán J, Cladera A, Oller E, Ribas C. Shear-flexural strength mechanical model for the design and assessment of reinforced concrete beams. *Struct Infrastruct Eng* 2015;11:1399–419. <https://doi.org/10.1080/15732479.2014.964735>."
- [4] "Park HG, Kang S, Choi KK. Analytical model for shear strength of ordinary and prestressed concrete beams. *Eng Struct* 2013;46:94–103. <https://doi.org/10.1016/j.engstruct.2012.07.015>."
- [5] "Collins MP, Bentz EC, Sherwood EG, Xie L. An adequate theory for the shear strength of reinforced concrete structures. *Mag Concr Res* 2008;60(9):635–50. <https://doi.org/10.1680/macr.2008.60.9.635>."
- [6] "Bažant ZP, Yu Q, Gerstle W, Hanson J, Ju JW. Justification of ACI 446 proposal for updating ACI code provisions for shear design of reinforced concrete beams. *Struct J* 2007;104:601–10."
- [7] "Choi KK, Park HG, Wight JK. Unified shear strength model for reinforced concrete beams - part I: development. *ACI St. J* 2007;104(2):142–52."
- [8] "Tureyen AK, Frosch RJ. Concrete shear strength: another perspective. *ACI Struct J* 2003;100(5):609–15."
- [9] "Zararis PD, Papadakis GC. Diagonal shear failure and size effect in RC beams without web reinforcement. *J Struct Eng* 2001;127(7):733–42. [https://doi.org/10.1061/\(ASCE\)0733-9445\(2001\)](https://doi.org/10.1061/(ASCE)0733-9445(2001))."
- [10] "Reineck KH. Ultimate shear force of structural concrete members without transverse reinforcement derived from a mechanical model. *ACI Struct J (SP-885)* 1991;88(5):592–602."
- [11] "Hsu T. Softened truss model theory for shear and torsion. *ACI Struct J* 1988;85(6):624–35."
- [12] "CEN European Committee for Standardization. Eurocode 2: design of concrete structures: part 1: general rules and rules for buildings. Brussels. CEN; 2002."
- [13] "FIB – International Federation for Structural Concrete. FIB Model Code for Concrete Structures 2010. Berlin: Verlag Ernst & Sohn; 2013. <http://doi.org/10.1002/9783433604090>."
- [14] "ACI-Committee-318. Building code requirements for structural concrete and commentary. USA: ACI; 2008. ISBN 978-0-87031-264-9."
- [15] "Pujol M. Refuerzo a cortante de estructuras de ormgión armado con laminados de polímeros reforzados con fibras (FRP). Verificación experimental PhD Thesis Universitat Politècnica de Catalunya; 2018."
- [16] "C. Giaccio, R. Al-Mahaidi, and G. Taplin, "Experimental study on the effect of flange geometry on the shear strength of reinforced concrete T-beams subjected to concentrated loads," *Canadian Journal of Civil Engineering*, vol. 29, no. 6, pp. 911–918, 2002, doi: 10.1139/102-099."
- [17] "Placas A, Regan PE, Baker ALL. Shear failure of reinforced concrete beams. *J Amer Concr Inst* 1971;68:763–73."
- [18] "Pujol M, Oller E, Marí A. Contribution of external transverse strengthening with FRP laminates to the shear strength of T beams (in Spanish). Proceedings VI congress of the spanish concrete association (ACHE), Madrid, 3–5 June 2014. 2014."
- [19] "Ribas C, Cladera A. Experimental study on shear strength of beam-and-block floors. *Eng Struct* 2013;57:428–42. <https://doi.org/10.1016/j.engstruct.2013.10.001>."
- [20] "Ferguson PM, Thompson JN. Diagonal tension in t-bemas without stirrups. *ACI J Proc* 1953;49(3):665–75."
- [21] "Kani MW, Huggins MW, Kani G, Wittkopp RR. Kani on shear in reinforced concrete. Toronto, Canada: University of Toronto, Dept. of Civil Engineering; 1979. ISBN 0772770018, 9780772770011."
- [22] "Leonhardt F. Shear and torsion in prestressed concrete. London: Fédération Internationale de la Précontrainte, Cement & Concrete Association; 1970."
- [23] "M. Shoukry, Z. Mahmoud, M. Elnaggar, and M. Kamel, "Shear Strength of Fiber Reinforced Concrete (FRC) Beams without Stirrups," *J. Eng. Res.*, pp. 0–0, Feb. 2023, doi: 10.21608/erjeng.2023.187401.1145."
- [24] "mahmoud Abdelaziz, E. Etman, M. Hussien, and N. Kasem, "Enhancing the behavior of R.C. Continuous-Defected Slabs Using Strain-Hardening Cementitious Composites (SHCC)," *J. Eng. Res.*, vol. 7, no. 2, pp. 0–0, May 2023, doi: 10.21608/erjeng.2023.212986.1182."
- [25] "ACI-ASCE Committee 426. The shear strength of reinforced concrete members. *ACI J Proc* 1973;70:1091–187."
- [26] "R. N. Swamy and S. A. Qureshi, "An ultimate shear strength theory for reinforced concrete T-beams without web reinforcement," *Matériaux et Constructions*, vol. 7, no. 3, pp. 181–189, 1974, doi: 10.1007/BF02473833."
- [27] "Hoang CL. Shear strength of non-shear reinforced concrete elements: Part 1- Statically indeterminate beams. Research Report, Department of Structural Engineering and Materials. Lyngby, Denmark: Technical University of Denmark; 1997."
- [28] "Kotsovos MD, Bobrowski J, Eibl J. Behaviour of reinforced concrete T-beams in shear. *Struct Eng Part B R&D Q* 1987;65B:1–10."
- [29] "Zararis IP, Karaveziroglou MK, Zararis PD. Shear strength of reinforced concrete T-beams. *ACI Struct J* 2006;103:693–700."
- [30] "J. M. Bairan Garcia and A. R. Mari Bernat, "Bairán JM, Mari AR. Coupled model for the non-linear analysis of anisotropic sections subjected to general 3D loading. Part 1: theoretical formulation. *Comput Struct* 2006;84(31–32):2254–63. <https://doi.org/10.1016/j.compstruc.2006.08.036>," *Computers and Structures*, vol. 84, no. 31–32, pp. 2254–2263, 2006, doi: 10.1016/j.compstruc.2006.08.036."



- [31] “Swamy RN, Qureshi SA. An ultimate shear strength theory for reinforced concrete Tbeams without web reinforcement. *Matér Constr* 1974;7:181–9. <https://doi.org/10.1007/BF02473833>.”
- [32] “Ribas C, Cladera A. Mechanical model for calculating the shear strength of beam-and-block floors. *Informes de la Construcción* 2014;66(1):1–10.”
- [33] A. Cladera, A. Marí, C. Ribas, J. Bairán, and E. Oller, “Predicting the shear–flexural strength of slender reinforced concrete T and I shaped beams,” *Eng. Struct.*, vol. 101, pp. 386–398, Oct. 2015, doi: 10.1016/j.engstruct.2015.07.025.
- [34] “Li YA, Hsu TTC, Hwang SJ. Shear strength of prestressed and non-prestressed concrete beams. *Concrete International*, American Concrete Institute; 2017. p. 53–7.” [Online]. Available: https://www.researchgate.net/publication/326368196_Shear_Strength_of_Prestressed_and_Nonprestressed_Concrete_Beams.
- [35] A. Ayensa, E. Oller, B. Beltrán, E. Ibarz, A. Marí, and L. Gracia, “Influence of the flanges width and thickness on the shear strength of reinforced concrete beams with T-shaped cross section,” *Eng. Struct.*, vol. 188, pp. 506–518, Jun. 2019, doi: 10.1016/j.engstruct.2019.03.057.
- [36] “Belletti B, Damoni C, Hendriks MAN, Den Uijl JA. Non-linear finite element analyses of existing reinforced concrete bridge beams. *IABSE Symposium Report*, vol. 99 no. 7. 2013.p. 1631–8.”
- [37] J. Navarro Gregori, P. Miguel Sosa, M. A. Fernández Prada, and F. C. Filippou, “A 3D numerical model for reinforced and prestressed concrete elements subjected to combined axial, bending, shear and torsion loading,” *Engineering Structures*, vol. 29, no. 12. pp. 3404–3419, 2007, doi: 10.1016/j.engstruct.2007.09.001.
- [38] “Dassault Systèmes. Abaqus software [accessed 28 June 2018]. <https://www.3ds.com/products-services/simulia/products/abaqus/>; 2018.”
- [39] “Choi, K.-K., Park, H.-G., Wight, J.K. Unified shear strength model for reinforced concrete beams - Part I: Development (2007) *ACI Structural Journal*, 104 (2), pp. 142-152. Cited 77 times.”
- [40] U. M. D. E. C. D. E. Los, “ABAQUS (2012) Analysis User’s Manual. Version 6.12, Dassault Systemes Simulia, Inc.,” doi: <https://www.3ds.com/products-services/simulia/products/abaqus/>.
- [41] “ACI Committee 318 (2019). *Building Code Requirements for Structural Concrete (ACI 318-19) and Commentary (ACI 318R-19)*. American Concrete Institute, Farmington Hills, MI, 519 pp.”